Experimental investigation and a novel analytical solution of turbulent boundary layer flow over a flat plate in a wind tunnel

Shahmohamadi, Hamed; Rashidi, Mohammad Mehdi

DOI:
10.1016/j.ijmecsci.2017.08.043

Document Version
Peer reviewed version

Citation for published version (Harvard):
Shahmohamadi, H & Rashidi, MM 2017, 'Experimental investigation and a novel analytical solution of turbulent boundary layer flow over a flat plate in a wind tunnel', *International Journal of Mechanical Sciences*, vol. 133, pp. 121-128. https://doi.org/10.1016/j.ijmecsci.2017.08.043

Experimental Investigation and a Novel Analytical Solution of Turbulent Boundary Layer Flow over a Flat Plate in a Wind Tunnel

Hamed Shahmohamadi , Mohammad Mehdi Rashidi

PII: S0020-7403(17)30478-2
DOI: 10.1016/j.ijmecsci.2017.08.043
Reference: MS 3894

To appear in: *International Journal of Mechanical Sciences*

Received date: 26 February 2017
Revised date: 1 August 2017
Accepted date: 20 August 2017

Please cite this article as: Hamed Shahmohamadi , Mohammad Mehdi Rashidi , Experimental Investigation and a Novel Analytical Solution of Turbulent Boundary Layer Flow over a Flat Plate in a Wind Tunnel, *International Journal of Mechanical Sciences* (2017), doi: 10.1016/j.ijmecsci.2017.08.043

Highlights

- The fluid mechanics of incompressible turbulent boundary layers air flow over a flat plate is investigated.
- Thin-Oil-film technique is used to determine skin friction of the plate.
- Reynolds averaged Navier-Stokes equations are normalized by appropriate similarity transformations.
- Variational Iteration Method (VIM) was applied for finding the analytical solution.
- New correlations for skin friction coefficient and boundary layer thickness of turbulent flow over flat plate are proposed.

Experimental Investigation and a Novel Analytical Solution of Turbulent Boundary Layer Flow over a Flat Plate in a Wind Tunnel

Hamed Shahmohamadi [1*], Mohammad Mehdi Rashidi [2]

[1]*Department of Mechanical and Aerospace Engineering, University of California at Los Angeles, Los Angeles, CA 90095, USA*

[*]hamedshah@ucla.edu

[2]*Department of Civil Engineering, School of Engineering, University of Birmingham, Birmingham, UK*

Abstract

The fluid mechanics of incompressible turbulent boundary layers air flow over a flat plate is investigated using an open-ended suction wind tunnel. The wall shear stress is measured by a distinct method using Thin-Oil-film technique in order to determine skin friction of the plate. On theoretical side, the governing partial differential equations are transformed to an ordinary differential equation with inconsistent coefficients using similarity variables and they are solved by variational iteration method. The distribution of the velocity, friction coefficient and thickness of the boundary layer are obtained analytically and experimentally, and compared with the previously reported results, where good agreements are observed. New correlations for skin friction coefficient and boundary layer thickness of turbulent flow over flat plate are proposed.

Keywords: Turbulent flow; Boundary layer; Skin friction; Wind tunnel; Thin-oil-film technique; Variational Iteration Method (VIM)

1. Introduction

In spite of the many endeavours and experimental works undertaken in the past several years, the effect of turbulent boundary layers flow on the aerodynamics forces is still not fully understood. The air flow on turbulent boundary layers is highly important for various engineering applications such as aerodynamics and design of building and structures, and also concerned

with the dispersion of natural ventilation and heat transfer between the ground surface and the atmosphere. There are some improved relations for certain situations and mathematical models, for example implemented in computational methods in literature. However, there is not as much research done on the manipulation of the boundary layer since the 'discovery' of the boundary layer. This can be of interest for studies on efficiency or drag of wings of aircrafts or blades of wind turbines.

In the past few years, different experiments have been carried out by many researchers for measuring skin friction and drag force in wind tunnels to grasp the various aerodynamic effects in real environment. Maruyama [1] used a floating element in the water bath. The floating element used in his experiment was not connected to the floor of the wind tunnel. Latter, Mochizuki et al [2] installed a floating element to a mechanical device in the wind tunnel to direct measurement of the wall shear stress. Gillies et al [3] measured drag force on individual obstacles on a load cell. They used the shear stress partitioning model for predicting the amount of surface shear stress, given knowledge of the stated input parameters for the patches of roughness in their experiment. Cheng et al [4] conducted the experiment using an oil bath with a raft. They found surface shear stress about 25% greater than the measured Reynolds shear stress in the inertial sub-layer over the surfaces. They concluded that no constant stress region and extrapolation of the shear stress profiles in the inertial sub-layer to the zero-plane displacement provided a much better estimate of the surface shear stress. Buccolieri et al [5] measured drag force in the wind tunnels with a standard load cell. Fernholz et al [6] introduced a new developments and applications of skin-friction measuring techniques based on the oil-film interferometry. The oil-film interferometry technique could be applied to assess the shear stress and skin friction, and it has been proved scientifically and technically.

The configuration of turbulent boundary layer flow is very complicated, irregular and random. The boundary layer over a flat plate can also be considered as inner and outer layers with their own specific scaling and scaling between Wind Tunnels [7, 8]. In fact, the boundary layer velocity profile of turbulent flow over a flat plate (zero pressure gradients) has a larger velocity gradient at the wall since it is much fuller than the one in the laminar flow. This leads to have greater skin friction along the surface in the turbulent flow. In addition, a turbulent boundary layer on a flat plate with $\frac{\partial \mathrm{u}}{\partial \mathrm{t}} = 0$ is used broadly for the intention of turbulence research as an

important approximation for many problems in engineering. For instance, the boundary layer on an airplane fuselage in cruise conditions is very similar to the flat plate boundary layer. Turbulent boundary layer flow over a flat plate is also one of the most prevalent phenomena which befall in the blades of turbomachinery, rotary compressors and computing the friction force on lifting fuselage and surfaces.

A turbulent flow is called self-similar when all or some of its statistical properties are dependent to the particular combination of independent variables [9]. Therefore, self-similar flow depends on smaller number of variables. It is evident that dealing with this type of flows is much easier. Self-similar boundary layer is a worthwhile phenomenon that simplifies the solution and helps to better understanding of the boundary layer and experimental results. Townsend [10] introduced the self-similarity solution in turbulent flow as the symbol of a dynamic equilibrium. Wolfshtein [11] carried out a practicability study on the existence of self-similar solution for the 2-D incompressible turbulent boundary layer. Mellor and Gibson [12] demonstrated that self-similarity may be attained when free stream velocity is expressed as a function of longitude coordinates. Clauser [13] investigated experimentally on a desirable pressure gradient which generates a self-similarity turbulent boundary layer. In his study, a constant dimensionless pressure gradient was introduced as a condition for self-similarity of boundary layer.
Blasius [14] introduced a technique called “similarity solution” to reduce the partial differential equations (PDEs) to ordinary differential equations (ODEs) in boundary layer problems. This primitive study of Blasius became a basis for simplifying complex turbulent equations. Since turbulence is a sophisticated phenomenon and its analysis and precise identification is not routine, many researchers have tried to discover a similarity solution to simplify the solution process [15-17].

In recent decades, numerical approaches have been developed significantly. However, owing to some limitations [18], many researchers [19-22] have been fascinated by analytical solutions as alternative ways. Perturbation methods are one of the most recognized techniques which have been widely used by scientists in different areas of science and engineering [23]. However, these methods are suffering from the lack of dependency upon small and large physical variables. Hence, they are not capable to apply to some of strongly nonlinear problems. Consequently, non-perturbation methods such as VIM [24-27] exposed to remove the dependency to small and large

parameters. The VIM can be used in a direct way without using linearization, perturbation or restrictive assumptions.

The work presented in this paper is on experimental and analytical investigation of turbulent boundary layer air flow over a flat plate. A wind tunnel is used to beget turbulent air flow on the flat plate. Thin-Oil-film technique is used to measure the wall shear stress in order to calculate the skin friction on the plate. On the analytical side, the similarity variables of turbulent boundary layer flow over a flat plate are applied to collapse the partial differential equations (PDEs) into an ordinary differential equations (ODEs) one. Turbulence viscosity appears in the equations using Reynolds decomposition. Finally, the obtained equations are solved analytically by VIM. The main advantage of this method is its independency from upstream and downstream characteristics of air flow. Moreover, two novel expressions for the boundary layer thickness and friction coefficient are reported which were in good agreements with current experimental data.

2. Experimental Method

2.1. Test facility

A schematic of the test facility used for the experiment is shown in figure 1. The test setup consists of a wind tunnel, a camera, a beam-splitter, a lamp, a diffuser, optical glass (SF11) as a flat plate, a flow loop and data acquisition system. The experiments were conducted in a wind tunnel having a flow cross-section of 560 mm × 320 mm near the testing area. Flow in the tunnel is induced by a 10 HP centrifugal blower resulting in an air velocity up to 52 m/s. Flow straighteners are used at the inlet of the wind tunnel for uniform flow distribution. The velocity in the wind tunnel is measured using a pitot tube installed in the unobstructed flow area. Also measured are the air temperature and static pressure before the test section. Air density is calculated using the measured air temperature and pressure. The test is carried out at four different Reynolds numbers (0.1, 0.5, 1 and 5 million) and low Mach numbers (below 0.2).

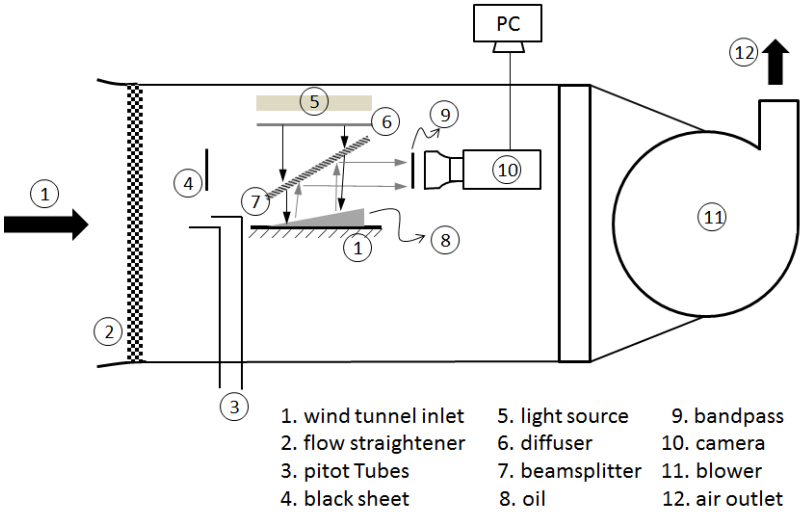

Fig. 1. Schematic of the test facility with different components.

2.2.Thin-Oil-film techniques

The oil-film interferometry method is based on the comportment of an oil film (normally less than 10 μm) when shear stress function on it. Applying the thin film interference to determine the oil film thickness for the first time was introduced by Tanner and Blows [28]. Skin friction would be gained by determining the wall shear stress in the wind tunnel. This means Thin- Oil-film technique is an indirect method for measuring skin friction or drag force. Therefore, it is necessary to have the correlation between the wall shear stress and the thickness of oil film on the wall. Once the oil on the smooth plate is exposed in the air flow inside the wind tunnel, a wedge shape film would be formed (figure 2).

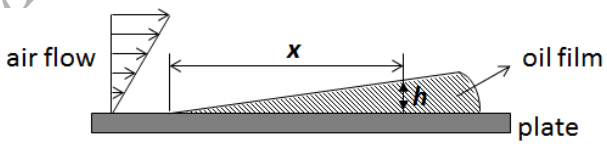

Fig .2. Schematic of stream wise cross-section of the oil film on the plate.

The shear stress would be uniform since the oil flow is considered two dimensional. As a result of small film thicknesses, the gravity effect, surface tension and the pressure gradient can be

neglected. Thus, the correlation between the wall shear stress and local oil thickness can be written as [29]:

$$\tau_w = \frac{\mu_{oil} x}{ht}, \tag{1}$$

where, τ_w is the wall shear stress, x is the displacement of oil, μ_{oil} is the viscosity of oil, t is the time and h is the local film thickness. The light source here is a high pressure mercury vapor lamp and it orients the light directly on the film with an angle of θ. As stated by the interferometry axiom, there are two types of reflected lights. One is reflected off the oil surface and the other after penetrating the oil, is reflected off the wall. As a result of interfering two reflected beams with each other, dark and bright fringes are formed as shown in figure 3. The minute film thickness of oil means the two reflected beams have different path lengths. If the beam reflected from the bottom plate undergoes a 180° phase reversal (as beams demonstrated in figure 3(a)) where the path difference is an even multiple of λ/2 (λ is the wavelength), the reflected waves from both surfaces interfere to cancel each other. If the beam reflected from the bottom plate undergoes in phase (as beams displayed in figure 3(b)) where the path difference is an odd multiple of λ/2, the two reflected waves reinforce each other.

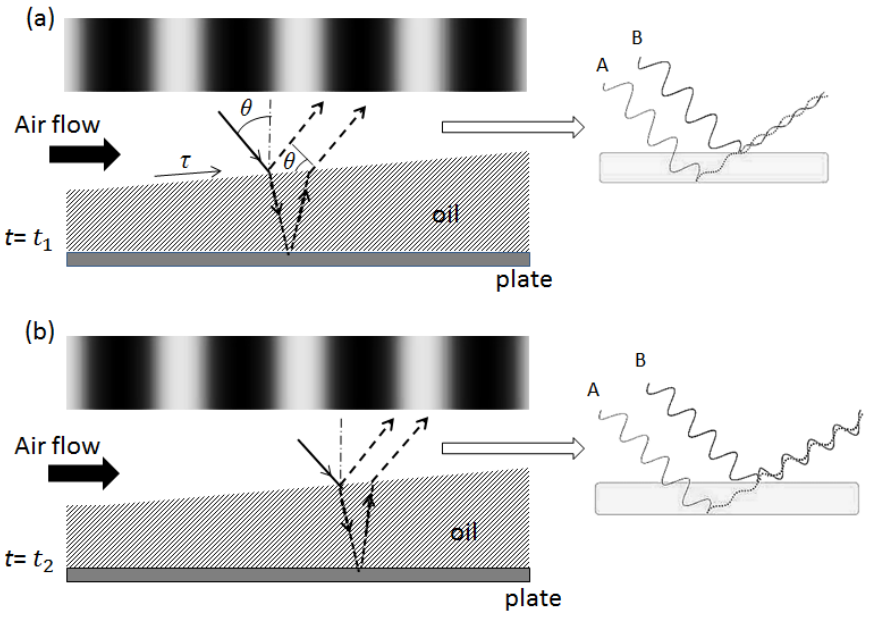

Fig. 3. (a) Destructive interference resulting dark fringe (reflected waves 180° out of phase), (b) Constructive interference resulting bright fringe (reflected waves in phase).

According to the interference optics principle, the film thickness can be written as [28]:

$$h = \frac{\lambda\varphi}{4\pi\sqrt{n_{oil}^2 - n_{air}^2 \sin^2(\theta)}}, \tag{2}$$

in which φ is the phase shift (difference) between the waves in radians n_{oil} and n_{air} are the refractive indices of oil and air respectively and λ is the wavelength of the incident light.

After defining the wall shear stress, the skin friction can be obtained as follows:

$$C_f = \frac{\tau_w}{\frac{1}{2}(\rho U_\infty^2)}, \tag{3}$$

where ρ is the density and U_∞ is the free stream velocity.

3. Mathematical Modeling

3.1. Governing equations

An incompressible turbulent flow over a flat plate with no pressure gradient is considered here. Cartesian coordinates x and y are aligned parallel and perpendicular to the wall respectively as shown in figure 4. Since the flow is turbulent, every velocity and pressure terms are quickly altering random functions of time and space due to the fluctuations. The Reynolds averaged Navier-Stokes (RANS) equations are considered for a two dimensional turbulence flow to determine the flow fields as expressed bellow [9]:

$$\frac{\partial\bar{u}}{\partial x} + \frac{\partial\bar{\upsilon}}{\partial y} = 0, \tag{4}$$

$$\bar{u}\frac{\partial\bar{u}}{\partial x} + \bar{\upsilon}\frac{\partial\bar{u}}{\partial y} = \frac{\partial}{\partial y}(\nu\frac{\partial\bar{u}}{\partial y} - \overline{u'\upsilon'}), \tag{5}$$

where $\bar{u}$ and $\bar{\upsilon}$ are the components of the velocity in x and y direction, respectively, ν is the kinematic viscosity, and prime (') indicates the fluctuation terms of the velocities. The boundary conditions can be written as:

$$u = \upsilon = 0 \quad \text{at} \quad y = 0,$$
$$u = U_\infty \quad \text{at} \quad y \to \infty. \tag{6}$$

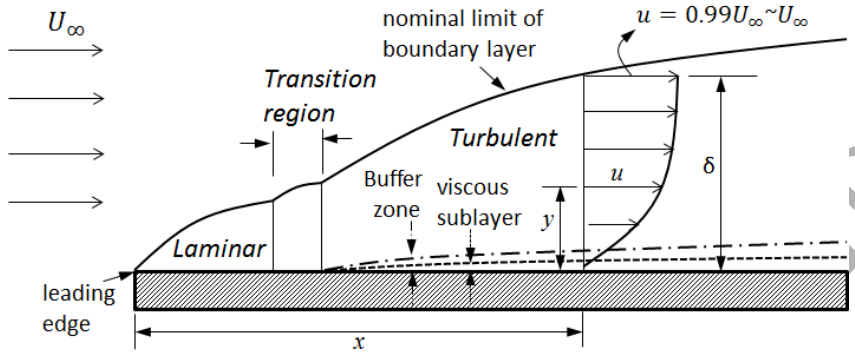

Fig. 4. Turbulent boundary layer over a flat plate.

In equation (5), Reynolds stress term can be expressed as [30]:

$$-\overline{u'\upsilon'} = \nu_t(y)\frac{\partial \overline{\upsilon}}{\partial y}, \tag{7}$$

where $\nu_t(y)$ is the turbulence eddy viscosity. Substituting equation (7) into equation (5) gives:

$$\overline{u}\frac{\partial \overline{u}}{\partial x} + \overline{\upsilon}\frac{\partial \overline{u}}{\partial y} = \nu\frac{\partial^2 \overline{u}}{\partial y^2} + \frac{\partial}{\partial y}(\nu_t \frac{\partial u}{\partial y}). \tag{8}$$

By applying Prandtl mixing length [30], the turbulence eddy viscosity can be written in the following form:

$$\nu_t = l_m^2 \frac{\partial \overline{u}}{\partial y}, \tag{9}$$

in which l_m is the Prandtl mixing length. The stream function is described as bellow:

$$\psi = U_\infty g(x) f(\eta), \tag{10}$$

where

$$\eta = \frac{y}{g(x)}. \tag{11}$$

It is worth mentioning that $g(x)$ and $f(\eta)$ are exclusive functions of x and η, respectively.

Considering the definition of the stream function, the equation (8) can be defined as:

$$\bar{u} = \frac{\partial \psi}{\partial y} = U_\infty f'(\eta), \tag{12}$$

$$\bar{v} = -\frac{\partial \psi}{\partial x} U_\infty g'(x)\left[\eta f'(\eta) - f(\eta)\right], \tag{13}$$

$$\frac{\partial \bar{u}}{\partial x} = -U_\infty \frac{g'(x)}{g(x)} \eta f''(\eta), \tag{14}$$

$$\frac{\partial \bar{u}}{\partial y} = \frac{U_\infty}{g(x)} f''(\eta), \tag{15}$$

$$\frac{\partial^2 \bar{u}}{\partial y^2} = \frac{U_\infty}{g^2(x)} f''(\eta), \tag{16}$$

$$\frac{\partial}{\partial y}(\nu_t \frac{\partial \bar{u}}{\partial y}) = \frac{U_\infty^2}{g^3(x)} \frac{\partial}{\partial \eta}\left(l_m^2 f''^2(\eta)\right). \tag{17}$$

By substituting equations (12)-(17) into equation (8) the generally self-similar equations can be written as follows:

$$f''' + \frac{U_\infty}{\nu} g'(x) g(x) f f'' + \frac{U_\infty}{\nu\, g(x)} \frac{\partial}{\partial \eta}\left(l_m^2 f''^2(\eta)\right) = 0. \tag{18}$$

The boundary layer over a flat plate can be considered as two divisions: inner and outer layers with their own specific scaling [30]. According to the experimental mixing length curve [31], the following correlation is considered:

$$\frac{1}{\delta^*} = \alpha \left(\frac{y}{\delta^*}\right)^n, \tag{19}$$

in which δ^* is the boundary layer thickness and α is a constant. Comparing Equation (19) to the experimental mixing length curve [31], gives:

$$l_m \propto y \qquad 0 < \frac{y}{\delta^*} < 0.1,$$
$$l_m \propto y^{1/2} \qquad 0.1 \le \frac{y}{\delta^*} < 1. \tag{20}$$

According to equation (19) we have:

$$l_m = \alpha\delta^* \left(\frac{y}{\delta^*}\right)^n \Rightarrow l_m^2 = \alpha^2 \delta^{*2} \left(\frac{y}{\delta^*}\right)^{2n}. \tag{21}$$

Thus, from equation (20), we can partition the solution domain into two sections:

I) At the vicinity of the surface where $n = 1,\ l \propto y \Rightarrow l = \kappa y$ ($\kappa = 0.41$) and equation (18) can be reduced to:

$$f''' + \frac{U_\infty}{\nu} g g' f f'' + \frac{U_\infty \kappa^2}{\nu} g \frac{\partial}{\partial \eta}(n^2 f''^2) = 0. \tag{22}$$

We consider the following assumption to make the coefficients independent of x in order to find a similarity solution

$$\frac{U_\infty}{\nu} g g' = 1 \quad \Rightarrow \quad g(x) = \sqrt{\frac{2\nu x}{U_\infty}}. \tag{23}$$

According to Equation (11), we have:

$$\eta_{99} = \frac{\delta^*}{g(x)}, \tag{24}$$

where $f'(\eta_{99}) = 0.99$. Substituting equation (24) into Equation (22) and using the definition of $\mathrm{Re}_\delta = U_\infty \delta^* / \nu$, equation (14) is simplified as:

$$f''' + f f'' + \kappa^2 \frac{\mathrm{Re}_\delta}{\eta_{99}} \frac{\partial}{\partial \eta}(\eta^2 f''^2) = 0, \tag{25}$$

with following boundary conditions:

$$f(0) = 0, \qquad f'(0) = 0. \tag{26}$$

II) Beyond the surface where $n = 0.5, y \geq 0.1\delta^*$ and equation (18) is reduced to:

$$f''' + ff'' + \alpha^2 \mathrm{Re}_\delta \frac{\partial}{\partial \eta}(\eta f''^2) = 0, \tag{27}$$

with the boundary condition as:

$$f'(\infty) = 1, \tag{28}$$

where the value of α can be found based on the work done by Anderson and Kays [31].

It is worth mentioning that the correlation between Re_δ and Re_x can be obtained as:

$$\mathrm{Re}_\delta = \frac{U_\infty \delta^*}{\nu} = \frac{U_\infty}{\nu}\eta_{99} g(x) = \frac{U_\infty}{\nu}\eta_{99}\sqrt{\frac{2\nu x}{U_\infty}} = \eta_{99}\sqrt{2\mathrm{Re}_x}. \tag{29}$$

Substituting equation (29) into equations (25) and (27) gives the ODE as follows:

$$f''' + 2\kappa^2\sqrt{2\mathrm{Re}_x}\eta^2 f''f''' + 2\kappa^2\sqrt{2\mathrm{Re}_x}\eta f''^2 + ff'' = 0 \quad for \quad 0 < \frac{y}{\delta^*} = \frac{\eta}{\eta_{99}} < 0.1, \tag{30a}$$

$$f''' + 2\alpha^2\eta_{99}\sqrt{2\mathrm{Re}_x}\eta f''f''' + \alpha^2\eta_{99}\sqrt{2\mathrm{Re}_x} f''^2 + ff'' = 0 \quad for \quad 0.1 \leq \frac{y}{\delta^*} = \frac{\eta}{\eta_{99}} < 1, \tag{30b}$$

with the boundary conditions:

$$f(0) = f'(0) = 0, f'(\eta_{99}) = 1. \tag{31}$$

After solving above equations, the friction coefficient can be represented as:

$$C_f = \frac{1}{2}\frac{\tau_w}{\rho U_\infty^2}, \ and \ \ \tau_w = \mu\frac{\partial u}{\partial y}\bigg|_{y=0} = \mu\frac{U_\infty}{g(x)} f''(\eta)\bigg|_{\eta=0} = \sqrt{\frac{\rho\mu U_\infty^3}{2x}} f''(0) \ \Rightarrow \ C_f = \frac{f''(0)}{\sqrt{2\mathrm{Re}_x}}, \tag{32}$$

in which μ and ρ are dynamic viscosity and density, respectively. In addition, based on equation (24) the boundary layer thickness can be expressed as:

$$\eta_{99}=\frac{\delta^*}{g(x)}=\frac{\delta^*}{\sqrt{\frac{2\nu.x}{U_\infty}}}\ \Rightarrow\ \frac{\delta^*}{x}=\eta_{99}\sqrt{\frac{2}{\mathrm{Re}_x}}. \tag{33}$$

3.2. Analytical approach

According to VIM [24], in order to solve (30a) and (30b) the correction functional can be constructed as:

$$\begin{aligned} f_{m+1}(\eta)=\ & f_m(\eta)+\int_0^\eta \lambda\left[\frac{\partial^3 f_m(\tau)}{\partial\tau^3}+2\kappa^2\sqrt{2\mathrm{Re}_x}\tau^2\left(\frac{\partial^2\tilde{f}_m(\tau)}{\partial\tau^2}\frac{\partial^3\tilde{f}_m(\tau)}{\partial\tau^3}\right)\right. \\ & \left.+2\kappa^2\sqrt{2\mathrm{Re}_x}\tau\left(\frac{\partial^2\tilde{f}_m(\tau)}{\partial\tau^2}\right)^2+\tilde{f}_m(\tau)\frac{\partial^2\tilde{f}_m(\tau)}{\partial\tau^2}\right] \quad for \quad 0<\frac{y}{\delta^*}=\frac{\eta}{\eta_{99}}<0.1, \end{aligned} \tag{34a}$$

$$\begin{aligned} f_{m+1}(\eta)=\ & f_m(\eta)+\int_0^\eta \lambda\left[\frac{\partial^3 f_m(\tau)}{\partial\tau^3}+2\alpha^2\eta_{99}\sqrt{2\mathrm{Re}_x}\tau\left(\frac{\partial^2\tilde{f}_m(\tau)}{\partial\tau^2}\frac{\partial^3\tilde{f}_m(\tau)}{\partial\tau^3}\right)\right. \\ & \left.+\alpha^2\eta_{99}\sqrt{2\mathrm{Re}_x}\left(\frac{\partial^2\tilde{f}_m(\tau)}{\partial\tau^2}\right)^2+\tilde{f}_m(\tau)\frac{\partial^2\tilde{f}_m(\tau)}{\partial\tau^2}\right] \quad for \quad 0.1\le\frac{y}{\delta^*}=\frac{\eta}{\eta_{99}}<1, \end{aligned} \tag{34b}$$

in which λ is the general Lagrangian multiplier and $\tilde{f}_m(\tau)$ is considered as restricted variation, i.e. $\delta\tilde{f}_m(\tau)=0$. To find the optimal value of λ, we have

$$\delta f_{m+1}(\eta)=\delta f_m(\eta)+\delta\int_0^\eta\lambda\left[\frac{\partial^3 f_m(\tau)}{\partial\tau^3}\right]d\tau \tag{35}$$

Making the above correction functional stationary, the following stationary conditions can be obtained:

$$1+\lambda''(\tau)\big|_{\tau=\eta}=0,\quad \lambda(\tau)\big|_{\tau=\eta}=0,\quad \lambda'(\tau)\big|_{\tau=\eta}=0,\quad \lambda'''(\tau)=0. \tag{36}$$

Thus, the Lagrange multiplier can be expressed as:

$$\lambda=-\frac{1}{2}(\tau-\eta)^2, \tag{37}$$

as a result, the following variational iteration formula can be obtained

$$f_{m+1}(\eta) = f_m(\eta) - \frac{1}{2}\int_0^\eta (\tau-\eta)^2 \left[\frac{\partial^3 f_m(\tau)}{\partial \tau^3} + 2\kappa^2 \sqrt{2\,\mathrm{Re}_x}\,\tau^2 \left(\frac{\partial^2 \tilde{f}_m(\tau)}{\partial \tau^2} \frac{\partial^3 \tilde{f}_m(\tau)}{\partial \tau^3} \right) \right.$$
$$\left. + 2\kappa^2 \sqrt{2\,\mathrm{Re}_x}\,\tau \left(\frac{\partial^2 \tilde{f}_m(\tau)}{\partial \tau^2} \right)^2 + \tilde{f}_m(\tau) \frac{\partial^2 \tilde{f}_m(\tau)}{\partial \tau^2} \right] \quad for \quad 0 < \frac{y}{\delta^*} = \frac{\eta}{\eta_{99}} < 0.1, \tag{38a}$$

$$f_{m+1}(\eta) = f_m(\eta) - \frac{1}{2}\int_0^\eta (\tau-\eta)^2 \left[\frac{\partial^3 f_m(\tau)}{\partial \tau^3} + 2\alpha^2 \eta_{99} \sqrt{2\,\mathrm{Re}_x}\,\tau \left(\frac{\partial^2 \tilde{f}_m(\tau)}{\partial \tau^2} \frac{\partial^3 \tilde{f}_m(\tau)}{\partial \tau^3} \right) \right.$$
$$\left. + \alpha^2 \eta_{99} \sqrt{2\,\mathrm{Re}_x} \left(\frac{\partial^2 \tilde{f}_m(\tau)}{\partial \tau^2} \right)^2 + \tilde{f}_m(\tau) \frac{\partial^2 \tilde{f}_m(\tau)}{\partial \tau^2} \right] \quad for \quad 0.1 \le \frac{y}{\delta^*} = \frac{\eta}{\eta_{99}} < 1. \tag{38b}$$

Now we should start with arbitrary initial approximations such that they satisfy the boundary condition. According to equations (30a) and (30b) and boundary condition of (31), the boundary conditions can be divided into two distinct boundary conditions. As a result, equation (31) would be expressed as:

$$f(0) = f'(0) = 0,\ f'(\frac{\eta_{99}}{10}) = a \quad for \quad 0 < \frac{y}{\delta^*} = \frac{\eta}{\eta_{99}} < 0.1, \tag{39a}$$

$$f(\frac{\eta_{99}}{10}) = b,\ f'(\frac{\eta_{99}}{10}) = a,\ f'(\eta_{99}) = 1 \quad for \quad 0.1 \le \frac{y}{\delta^*} = \frac{\eta}{\eta_{99}} < 1, \tag{39b}$$

in which a and b are dummy variables and can be determined by a continuity of equations (30a) and (30b) at the point of $\eta = \eta_{99}/10$. It is now straight-forward to choose power initial guesses:

$$f_0(\eta) = C_0 + C_1\eta + C_2 e^{-\eta} \quad for \quad 0 < \frac{y}{\delta^*} = \frac{\eta}{\eta_{99}} < 0.1, \tag{40a}$$

$$f_{0.1}(\eta) = C_3 + C_4\eta + C_5 e^{-\eta} \quad for \quad 0.1 \le \frac{y}{\delta^*} = \frac{\eta}{\eta_{99}} < 1, \tag{40b}$$

where C_{0-5} are constants and can be obtained by defined boundary conditions. We use the symbolic software MATHEMATICA to solve the integrality equations, (38a) and (38b), with the initial functions of (40a) and (40b), and successively obtain $f_1(\eta)$. In the same way, we can obtain $f_2(\eta)$, etc.

4. Results and Discussion

In current analytical solution, η_{99} ought to be characterized beforehand in order to analyze the turbulent boundary layer.

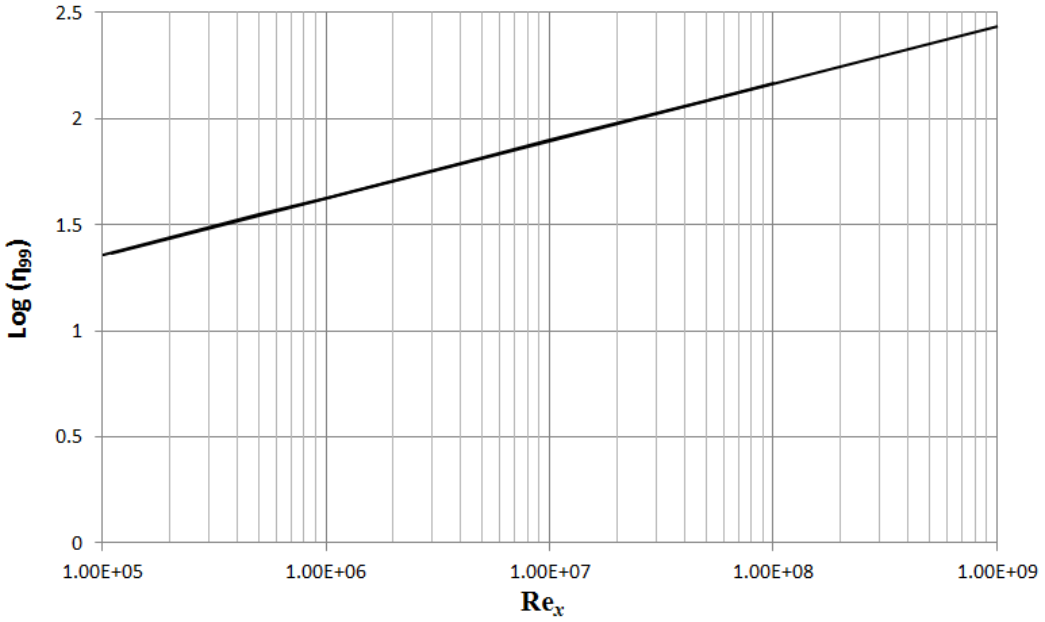

Fig. 5. Variation of the η_{99} at different Reynolds numbers.

Figure 5 demonstrates the results for the η_{99} which are gained in a transverse direction from the flat plate such that $U = 0.99U_{\infty}$. After determining η_{99} and once the equations (30a) to (30b) have been solved, the skin friction coefficient and the boundary layer thickness could be calculated from equations (32) and (33), respectively.

Variation of the skin friction coefficient C_f by Reynolds number is shown in Figure 6. The results in figure 6 are obtained from current analytical approach at Reynolds numbers in a range of 10^5 to 10^9. However, the measurements have been taken only at four different Reynolds number (0.1, 0.5, 1 and 5 million) based on capacity of the wind tunnel. This range can be extended to wider range in the experiment by redesigning the wind tunnel and using new facilities. Figure 6 is also illustrating the comparison of the current results and those obtained

from the well-established equations published by well-known authors in the literature. These include correlations of $C_f = 0.074\,\mathrm{Re}_x^{-0.2}$ introduced by Prandtl [32] in 1927, $C_f = 0.455[Log(\mathrm{Re}_x)]^{-2.58}$ presented by Prandtl and Schlichting [33] in 1934 and $C_f = 0.37[Log(\mathrm{Re}_x)]^{-2.584}$ suggested by Schultz and Grunov [34] in 1979. It is evident that there is good agreement between the results. Figure 6 shows that by increasing Reynolds number, C_f decreases. By applying curve fitting method to the current results, a new formula for C_f would be offered as:

$$C_f = 0.045\,\mathrm{Re}_x^{-0.16}. \tag{41}$$

According to the above equation, it is obvious that variations of local coefficient of friction in turbulent flow should be much lower than that of the laminar flow with relation of $C_f = 0.664\,\mathrm{Re}_x^{-0.5}$.

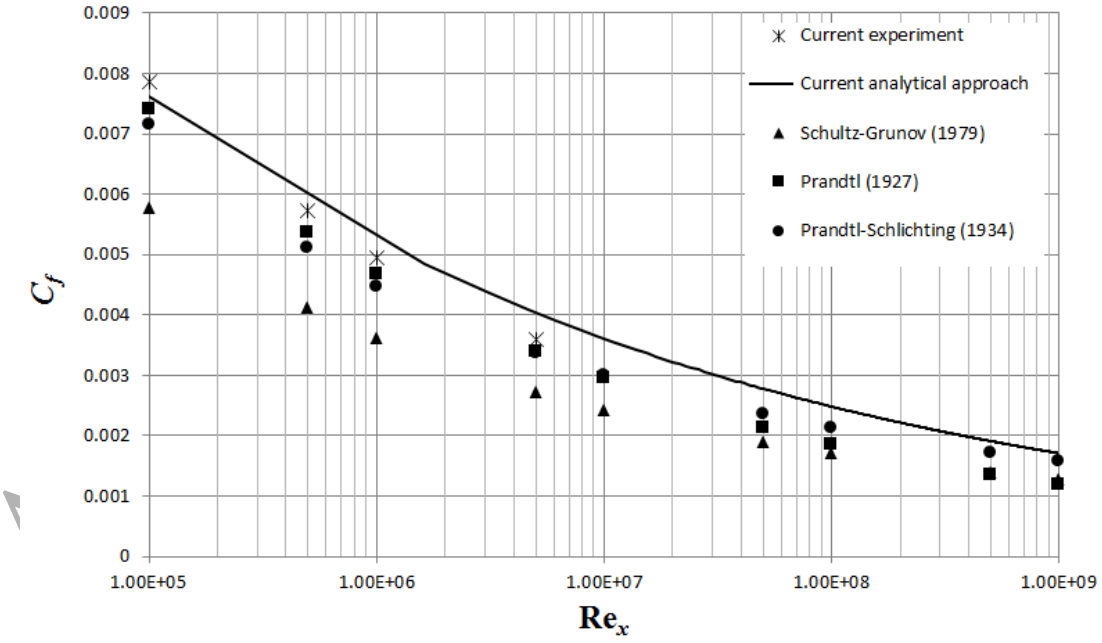

Fig. 6. Comparison of results for coefficient of friction obtained by current analysis with previously reported well-known correlations at different Reynolds number.

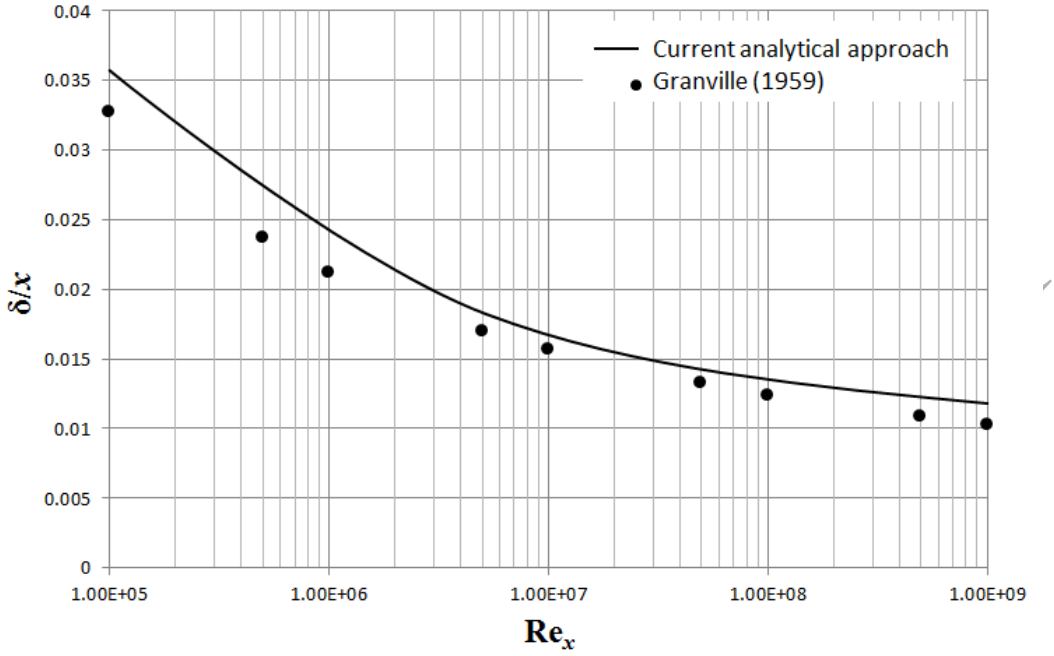

Fig. 7. Comparison of results for $\frac{\delta}{x}$ obtained by current analysis with previously reported well-known correlation at different Reynolds number.

Figure 7 shows the variations of $\frac{\delta}{x}$ by Reynolds number. The current results are also compared to those obtained by Granville [35]. In 1959, Granville introduced a correlation of $\frac{\delta}{x}=\frac{0.0598}{Log(\mathrm{Re}_x)-3.17}$ from velocity similarity laws for determination of the turbulent boundary-layer thicknesses of flat plate. According to his belief, a prediction of the thickness is a fundamental requirement in any studies of boundary layers but it was still surprising to find quoted in the literature Von Karman's 1/5-power law for smooth flat plates with turbulent boundary layers since this law is derived from 1/7-power velocity profiles and it has application to a limited range of Reynolds numbers, and since it is also based on pipe data it has only an approximate validity for flat plates. Based on current results, a new correlation can be introduced for the thickness of boundary layer using curve fitting method as:

$$\frac{\delta}{x}=0.169\,\mathrm{Re}_x^{-0.14}. \tag{42}$$

It is clear that, dependency of turbulent boundary layer thickness on the length of flat plate should be greater than that of the laminar boundary layer. By increasing the Reynolds number, the effects of transition region decreases and the analytical results becomes much closer to experimental ones. Deviation of velocity profile at low Reynolds number such 10^{-5} could be attributed to the transition region. That is why the overlap of the velocity profiles at the higher Reynolds number is much better and the accuracy of the results is high. As a result of figure 7, as Reynolds number increases, the thickness of turbulent boundary layer decreases.

The variation of dimensionless velocity profiles U/U_∞ versus η/η_∞ is displayed in Figure 8. As it can be seen in this figure, by gaining Reynolds number the transferred momentum between the core of the flow and the wall is accomplished, and hence the velocity gradient is increased at the vicinity of the plate.

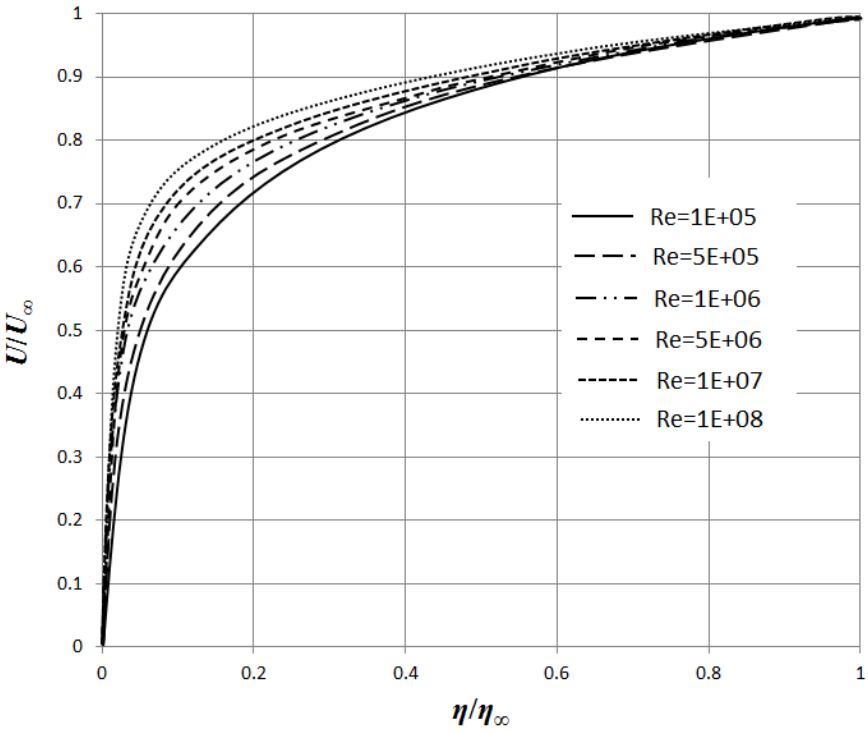

Fig. 8. Dimensionless velocity profile U/U_∞ versus η/η_∞ at different Reynolds number

5. Conclusion

A combined experimental and theoretical analysis of the turbulent boundary layers air flow over a flat plate was carried out. Thin-Oil-film technique was used as a new method to measure wall shear stress in order to determine skin friction of the flat plate in an open-ended suction wind tunnel. The test was performed at four different Reynolds numbers (0.1, 0.5, 1 and 5 million) and low Mach numbers (below 0.2).The detailed theoretical analysis comprises reduction of the Reynolds averaged Navier-Stokes differential equation from partial form to the ordinary form using similarity transformation and utilization of VIM for its novel analytical solution. The VIM was used in a direct way without using linearization, perturbation or restrictive assumptions. The method requires less computational work than existing approaches while supplying quantitatively reliable results. Good agreement was observed between current results and previously reported well-known ones. Finally, two new correlations for the friction coefficient and boundary layer thickness as functions of Reynolds number were suggested. The results exposed that the new introduced correlations can be used for wide range of the Reynolds number in different engineering applications.

Nomenclature

C_f	Skin-friction coefficient
L	Length of the plate
l_m	Prandtl mixing length
Re_x	Reynolds number based on x
Re_δ	Reynolds number based on Boundary layer thickness
t	Time
$\bar{u}$	Component of the velocity in x direction
$\bar{v}$	Component of the velocity in y direction
U_∞	Free stream velocity
x, y	Coordinates along and perpendicular to the plate

Greek Symbols

δ^*	Boundary layer thickness

η	Dimensionless variable
φ	Phase shift between the waves
λ	General Lagrangian multiplier
μ	Dynamic viscosity
ν	Kinematic viscosity
ν_t	Turbulent eddy viscosity
ρ	Density
τ_w	Wall shear stress (Pa)
∞	Free stream condition

Abbreviations

ODE	Ordinary Differential Equation
PDE	Partial Differential Equation
RANS	Reynolds Averaged Navier-Stokes
VIM	Variational Iteration Method

References

[1] T. Maruyama, Optimization of roughness parameters for staggered arrayed cubic blocks using experimental data, *Journal of Wind Engineering and Industrial Aerodynamics*, 46-47 (1993) 165-171.

[2] S. Mochizuki, T. Kameda, H. Osaka, Self-preservation of a turbulent boundary layer over d-type roughness, *Journal of Fluid Science and Technology*, 1 (2006) 24-35

[3] J.A. Gillies, W.G. Nickling, J. King, Shear stress partitioning in large patches of roughness in the atmospheric inertial sublayer, *Boundary-Layer Meteorology*, 122 (2007) 367-396.

[4] H. Cheng, P. Hayden, A.G. Robins, I.P. Castro, Flow over cube arrays of different packing densities, *Journal of Wind Engineering and Industrial Aerodynamics* 95 (2007) 715-740.

[5] R. Buccolieri, F. Sartoretto, A. Giacometti, S. Di Sabatino, L.S. Leo, B. Pulvirenti, M. Sandberg, H. Wigö, Flow and pollutant dispersion within the Canal Grande channel in Venice via CFD techniques, *13th International Conference on Harmonisation within Atmospheric Dispersion Modelling for Regulatory Purposes, Paris, France* (2010)

[6] H. H. Fernholz, G. Janke, M. Schober, P. M. Wagner, and D. Warnack. New developments and applications of skin-friction measuring techniques, *Measurement Science and Technology*, 7 (1996) 1396-1409.

[7] B. Rasuo, Scaling between Wind Tunnels–Results Accuracy in Two-Dimensional Testing, Transactions of the Japan Society for Aeronautical & Space Sciences, 55 (2012) 109-115.

[8] D. Damljanovic, J. Isakovic, B. Rasuo, T-38 Wind-Tunnel Data Quality Assurance Based on Testing of a Standard Model, Journal of Aircraft, AIAA, 50 (2013) 1141-1149.

[9] F.M. White, I. Corfield, Viscous fluid flow, *McGraw-Hill New York*, 2006.

[10] A.A. Townsend, The structure of turbulent shear flow, *Cambridge university press*, 1980.

[11] M. Wolfshtein, The self-similar turbulent boundary layer with injection, *International Heat Transfer Conference 13, Begel House Inc.*, 2006.

[12] G. Mellor, D. Gibson, Equilibrium turbulent boundary layers, Journal of Fluid Mechanics, 24 (1966) 225-253.

[13] F. Clauser, Turbulent boundary layers in adverse pressure gradients, *Journal of the Aeronautical Sciences*, 21 (1954) 91-108.

[14] H. Blasius, Grenzschichten in Flüssigkeiten mit kleiner Reibung, *Druck von BG Teubner*, 1907.

[15] T. Cebeci, A. Smith, Analysis of turbulent boundary layers, *NASA STI/Recon Technical Report A*, 75 (1974) 46513.

[16] R. Henkes, Scaling of the turbulent boundary layer along a flat plate according to different turbulence models, *International journal of heat and fluid flow*, 19 (1998) 338-347.

[17] G. Barenblatt, Scaling laws for fully developed turbulent shear flows. Part1. Basic hypotheses and analysis, *Journal of Fluid Mechanics*, 248 (1993) 513-520.

[18] H. Shahmohamadi, Analytic study on non-Newtonian natural convection boundary layer flow with variable wall temperature on a horizontal plate, *Meccanica*, 47 (2012), 1313-1323.

[19] W. Cai, M. Sen, K.T. Yang, Techniques of analysis for nonlinear transient flow in a pipe, *International Journal of Mechanical Sciences*, 54 (2012) 182-189.

[20] M. Turkyilmazoglu, Analytic approximate solutions of rotating disk boundary layer flow subject to a uniform suction or injection, *International Journal of Mechanical Sciences*, 52 (2010) 1735-1744.

[21] MM Rashidi, H Shahmohamadi, S Dinarvand, Analytic approximate solutions for unsteady two-dimensional and axisymmetric squeezing flows between parallel plates, *Mathematical Problems in Engineering*, 2008 (2008), ID: 935095

[22] MM Rashidi, H Shahmohamadi, Analytical solution of three-dimensional Navier–Stokes equations for the flow near an infinite rotating disk, *Communications in Nonlinear Science and Numerical Simulation* 14 (2009), 2999-3006

[23] J. Kevorkian, J.D. Cole, Perturbation Methods in Applied Mathematics, *Springer New York*, 2013.

[24] He, J. H., Variational iteration method—a kind of non-linear analytical technique: some examples, *International Journal of Non-Linear Mechanics*, 34 (1999) 699–708.

[25] H. Shahmohamadi, MM. Rashidi, VIM solution of squeezing MHD nanofluid flow in a rotating channel with lower stretching porous surface, *Advanced Powder Technology* 27 (2016), 171-178.

[26] H. Shahmohamadi, MM. Rashidi, A Novel Solution for the Glauert-Jet Problem by Variational Iteration Method-Padé Approximant, *Mathematical Problems in Engineering*, 2010 (2010) ID: 501476.

[27] MM. Rashidi, DD. Ganji, H. Shahmohamadi, Variational iteration method for two-dimensional steady slip flow in micro-channels, *Archive of Applied Mechanics*, 81 (2011), 1597-1605.

[28] L. H Tanner and L. G Blows. A study of the motion of oil films on surfaces in air flow, with application to the measurement of skin friction, *Journal of Physics E*, 9 (1976) 194-202.

[29] J. D. Murphy and R. V. Westphal. The laser interferometer skin-friction meter: A numerical and experimental study, *Journal of Physics E*, 19 (1986) 744-751.

[30] H. Schlichting, K. Gersten, Boundary-layer theory, *Springer Science & Business Media*, 2003.

[31] P. Andersen, W. Kays, R. Moffat, Experimental results for the transpired turbulent boundary layer in an adverse pressure gradient, *Journal of Fluid Mechanics*, 69 (1975) 353-375.

[32] L. Prandtl, The Generation of Vortices in Fluids of Small Viscosity, *The Aeronautical Journal*, 31 (1927) 718-741.

[33] L. Prandtl and H. Schlichting, Das Widerstandsgesetz rauher Platten. *Werft, Reederei, Hafen*, 21(1934) 649- 662.

[34] H. Schlichting, Boundary Layer Theory, *ISBN 0-07-055334-3*, (1979), 7th Edition.

[35] P. S. Granville, The determination of the local skin friction and the thickness of turbulent boundary layers from the velocity similarity laws, *Department of the Navy David Taylor Model Basin, Hydrodynamics Laboratory, Research and Development report*, (1959)

Graphical Abstract: